# Aberrant calcium signaling by transglutaminase-mediated posttranslational modification of inositol 1,4,5-trisphosphate receptors

Kozo Hamada[a,b,1], Akiko Terauchi[a,b], Kyoko Nakamura[b,c], Takayasu Higo[a,2], Nobuyuki Nukina[d,e], Nagisa Matsumoto[a], Chihiro Hisatsune[a], Takeshi Nakamura[b,3], and Katsuhiko Mikoshiba[a,b,1]

[a]Laboratory for Developmental Neurobiology, Brain Science Institute, Institute of Physical and Chemical Research (RIKEN), 2-1 Hirosawa, Wako, Saitama 351-0198, Japan; [b]Calcium Oscillation Project, International Cooperative Research Project–Solution Oriented Research for Science and Technology, Japan Science and Technology Agency, 4-1-8 Honcho, Kawaguchi, Saitama 332-0012, Japan; [c]Department of Physiology, Juntendo University Faculty of Medicine, 2-1-1 Hongo, Bunkyo-ku, Tokyo 113-8421, Japan; [d]Laboratory for Structural Neuropathology, Brain Science Institute, RIKEN, 2-1 Hirosawa, Wako, Saitama 351-0198, Japan; and [e]Department of Neuroscience for Neurodegenerative Disorders, Juntendo University Graduate School of Medicine, 2-1-1 Hongo, Bunkyo-ku, Tokyo 113-8421, Japan

Edited by Solomon H. Snyder, The Johns Hopkins University School of Medicine, Baltimore, MD, and approved August 19, 2014 (received for review May 27, 2014)

**The inositol 1,4,5-trisphosphate receptor ($IP_3R$) in the endoplasmic reticulum mediates calcium signaling that impinges on intracellular processes. $IP_3Rs$ are allosteric proteins comprising four subunits that form an ion channel activated by binding of $IP_3$ at a distance. Defective allostery in $IP_3R$ is considered crucial to cellular dysfunction, but the specific mechanism remains unknown. Here we demonstrate that a pleiotropic enzyme transglutaminase type 2 targets the allosteric coupling domain of $IP_3R$ type 1 ($IP_3R1$) and negatively regulates $IP_3R1$-mediated calcium signaling and autophagy by locking the subunit configurations. The control point of this regulation is the covalent posttranslational modification of the Gln2746 residue that transglutaminase type 2 tethers to the adjacent subunit. Modification of Gln2746 and $IP_3R1$ function was observed in Huntington disease models, suggesting a pathological role of this modification in the neurodegenerative disease. Our study reveals that cellular signaling is regulated by a new mode of posttranslational modification that chronically and enzymatically blocks allosteric changes in the ligand-gated channels that relate to disease states.**

allosteric regulation | $IP_3$ receptor | isopeptide bond | transamidation | deamidation

Ligand-gated ion channels function by allostery that is the regulation at a distance; the allosteric coupling of ligand binding with channel gating requires reversible changes in subunit configurations and conformations (1). Inositol 1,4,5-trisphosphate receptors ($IP_3Rs$) are ligand-gated ion channels that release calcium ions ($Ca^{2+}$) from the endoplasmic reticulum (ER) (2, 3). $IP_3Rs$ are allosteric proteins comprising four subunits that assemble a calcium channel with fourfold symmetry about an axis perpendicular to the ER membrane. The subunits of three $IP_3R$ isoforms ($IP_3R1$, $IP_3R2$, and $IP_3R3$) are structurally divided into three domains: the $IP_3$-binding domain (IBD), the regulatory domain, and the channel domain (3–6). Fitting of the IBD X-ray structures (7, 8) to a cryo-EM map (9) indicates that the IBD activates a remote $Ca^{2+}$ channel by allostery (8); however, the current X-ray structure only spans 5% of each tetramer, such that the mechanism underlying allosteric coupling of the IBD to channel gating remains unknown.

The $IP_3R$ in the ER mediates intracellular calcium signaling that impinges on homeostatic control in various subsequent intracellular processes. Deletion of the genes encoding the type 1 $IP_3R$ ($IP_3R1$) leads to perturbations in long-term potentiation/depression (3, 10, 11) and spinogenesis (12), and the human genetic disease spinocerebellar ataxia 15 is caused by haploinsufficiency of the $IP_3R1$ gene (13–15). Dysregulation of $IP_3R1$ is also implicated in neurodegenerative diseases including Huntington disease (HD) (16–18) and Alzheimer's disease (AD) (19–22). $IP_3Rs$ also control fundamental cellular processes—for example, mitochondrial energy production (23, 24), autophagy regulation (24–27), ER stress (28), hepatic gluconeogenesis (29), pancreatic exocytosis (30), and macrophage inflammasomes (31). On the other hand, excessive $IP_3R$ function promotes cell death processes including apoptosis by activating mitochondrial or calpain pathways (2, 17). Considering these versatile roles of $IP_3Rs$, appropriate $IP_3R$ structure and function are essential for living systems, and aberrant regulation of $IP_3R$ closely relates to various diseases.

Several factors such as cytosolic molecules, interacting proteins, and posttranslational modifications control the $IP_3$-induced $Ca^{2+}$ release (IICR) through allosteric sites in $IP_3Rs$. Cytosolic $Ca^{2+}$ concentrations strictly control IICR in a biphasic manner with activation at low concentrations and inhibition at higher concentrations. The critical $Ca^{2+}$ sensor for activation is conserved among the three isoforms of $IP_3$ and ryanodine receptors, and this sensor is located in the regulatory domain outside the IBD and the channel domain (32). A putative ATP regulatory region is deleted

## Significance

**Reversible and repetitive structural changes are essential for ligand-gated ion channels to mediate biological signaling. The inositol 1,4,5-trisphosphate receptor ($IP_3R$) assembles ligand-gated ion channels that mediate calcium signaling. $IP_3$ activates channels at a distance by reversible allosteric changes in the $IP_3R$ tetramer. Here we show a new mode of posttranslational modification that irreversibly blocks allosteric changes in the $IP_3R$. We identified an $IP_3R$-modifying enzyme as tissue transglutaminase that inhibits $IP_3R$ function by locking subunit configurations. This modification chronically impaired calcium signaling and autophagy regulation in living cells, and up-regulated modification was observed in Huntington disease models. To our knowledge, this is the first demonstration of transglutaminase-catalyzed posttranslational modification in ligand-gated channel allostery and provides a new framework for enzymatic regulation of allostery.**

Author contributions: K.H. designed research; K.H., A.T., K.N., T.H., N.M., and C.H. performed research; K.H., N.N., and K.M. contributed new reagents/analytic tools; K.M. supervised the project; K.H. and T.N. analyzed data; and K.H. wrote the paper.

The authors declare no conflict of interest.

This article is a PNAS Direct Submission.

[1]To whom correspondence may be addressed. Email: mikosiba@brain.riken.jp or hamada@brain.riken.jp.

[2]Present address: Laboratory for Cognitive Brain Mapping, Brain Science Institute, Institute of Physical and Chemical Research (RIKEN), 2-1 Hirosawa, Wako, Saitama 351-0198, Japan.

[3]Deceased July 23, 2006.

This article contains supporting information online at www.pnas.org/lookup/suppl/doi:10.1073/pnas.1409730111/-/DCSupplemental.

in *opisthotonos* mice, and IICR is also regulated by this mutation in the regulatory domain (33). Various interacting proteins, such as cytochrome *c*, Bcl-2-family proteins, ataxin-3, huntingtin (Htt) protein, Htt-associated protein 1A (HAP1A), and G-protein–coupled receptor kinase-interacting protein 1 (GIT1), target allosteric sites in the carboxyl-terminal tail (3–5). The regulatory domain and the carboxyl-terminal tail also undergo phosphorylation by the protein kinases A/G and B/Akt and contain the apoptotic cleavage sites for the protease caspase-3 (4, 5). These factors allosterically regulate $IP_3R$ structure and function to control cellular fates; therefore, understanding the allosteric coupling of the IBD to channel gating will elucidate the regulatory mechanism of these factors.

Transglutaminase (TG) catalyses protein cross-linking between a glutamine (Gln) residue and a lysine (Lys) residue via an $N^{\varepsilon}$-(γ-glutamyl)lysine isopeptide bond (34, 35). TG type 2 (TG2) is a $Ca^{2+}$-dependent enzyme with widespread distribution and is highly inducible by various stimulations such as oxidative stress, cytokines, growth factors, and retinoic acid (RA) (34, 35). TG2 is considered a significant disease-modifying factor in neurodegenerative diseases including HD, AD, and Parkinson's diseases (PD) (34, 36–45) because TG2 might enzymatically stabilize aberrant aggregates of proteins implicated in these diseases—that is, mutant Htt, β-amyloid, and α-synuclein; however, the causal role of TG2 in $Ca^{2+}$ signaling in brain pathogenesis has been unclear. Ablation of TG2 in HD mouse models is associated with increased lifespan and improved motor function (46, 47). However, TG2 knockout mice do not show impaired Htt aggregation, suggesting that TG2 may play a causal role in these disorders rather than TG2-dependent cross-links in aberrant protein aggregates (47, 48).

In this study, we discovered a new mode of chronic and irreversible allosteric regulation in $IP_3R1$ in which covalent modification of the receptor at Gln2746 is catalyzed by TG2. We demonstrate that up-regulation of TG2 modifies $IP_3R1$ structure and function in HD models and propose an etiologic role of this modification in the reduction of neuronal signaling and subsequent processes during the prodromal state of the neurodegenerative disease.

## Results

**Identification of an $IP_3R1$-Modifying Enzyme as TG.** In exploring a new allosteric mechanism of $IP_3R$ tetramers, we developed an agarose gel electrophoresis (AGE) system that can evaluate the large quaternary structure of $IP_3R1$ (>1 MDa) (Fig. 1 *A* and *B*). We found that the incubation of $IP_3R1$ with brain cytosol resulted in cross-linking of the $IP_3R1$subunits (Fig. 1*C*), indicating the existence of an endogenous cross-linking enzyme in the brain. We fractionated the cross-linking activity using chromatography (Fig. S1 *A*–*C*). The $Ca^{2+}$ dependence, elution profile of the activity, and inhibition with cystamine led us to postulate that the cross-linking might be catalyzed by a TG, most likely TG2 (34, 49).

The direct cross-linking of $IP_3R1$ by TG2 was confirmed using purified $IP_3R1$ and TG2 (Fig. S1*D*). To examine the role of TG2 in the cross-linking of $IP_3R1$, we silenced TG2 expression using siRNA in HeLa cells. TG2 knockdown completely abolished the in vitro cross-linking activity in HeLa cell lysates (Fig. 1*D*), indicating that TG2 is essential for the cross-linking of $IP_3R1$. In contrast, induction of TG2 expression by RA enhanced the cross-linking activity in HeLa cells (Fig. S1*E*). Similar cross-linking was observed in living cells including human neuroblastoma (SH-SY5Y) and human glioblastoma (U87-MG) cells (Fig. 1*E*). These results support the conclusion that $IP_3R1$ is an endogenous substrate of TG2 in living cells.

**TG2 Inhibits $IP_3R$-Mediated $Ca^{2+}$ Release.** The AGE analysis revealed that TG2 modifies the $IP_3R1$ structure; therefore, we examined whether TG2 regulates $IP_3R1$ function. We measured IICR using P2/P3 vesicles and found that purified TG2 inhibited IICR in

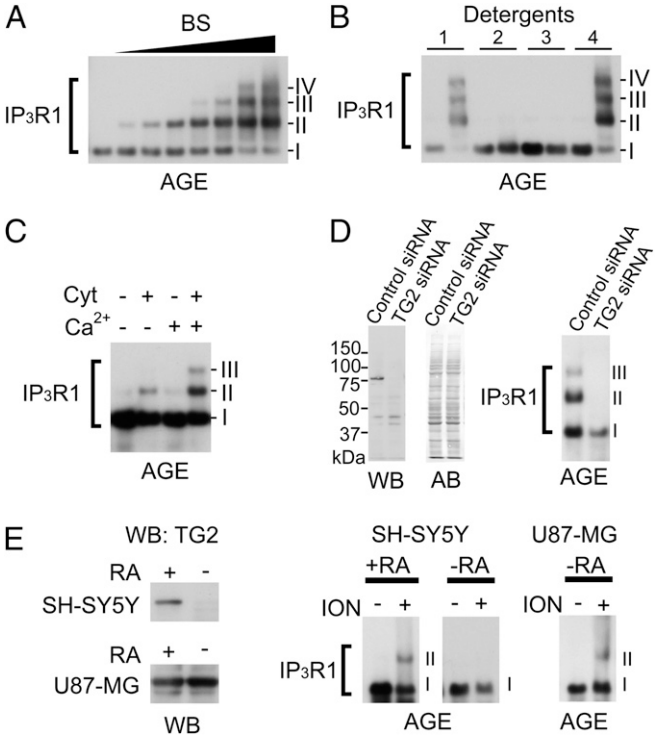


**Fig. 1.** Identification of an $IP_3R1$-modifying enzyme as TG. (*A*) Detection of cross-linked $IP_3R1$ by AGE. $IP_3R1$ subunits were cross-linked by the chemical cross-linker bis[sulfosuccinimidyl] suberate (BS). Roman numerals indicate cross-linked subunits observed by AGE; $IP_3R1$ sizes were compared with the thyroglobulin monomer (335 kDa) and dimer (670 kDa). (*B*) $IP_3R1$ (left lane) pretreated with Triton X-100 (*1*), Zwittergent 3–14 (*2*), SDS (*3*), or no detergent (*4*) was cross-linked with BS (right lane), indicating the oligomeric status (97). (*C*) Endogenous activity of $Ca^{2+}$-dependent cross-linking between $IP_3R1$ subunits in the brain cytosol (Cyt). (*D*) Cross-linking activity in HeLa cells pretreated with control siRNA or TG2 siRNA for 48 h. Western blots (WBs) with αTG2 and amido black (AB) staining show the cellular levels of TG2 and total proteins, respectively. (*E*) TG2 expression levels in SH-SY5Y or U87-MG cells treated with RA or DMSO. The *Right* panels show cross-linking of $IP_3R1$ by 10 μM ionomycin (ION) in human SH-SY5Y or U87-MG cells, as revealed by AGE.

a dose-dependent manner, without altering ATP-dependent $Ca^{2+}$ uptake or the total pool of $Ca^{2+}$ (Fig. 2*A*). The inhibitory effects were not observed using boiled TG2 or *N*-ethylmaleimide (NEM)-treated TG2, indicating that the catalytic activity of TG2 was required for inhibition (Fig. 2*A*).

To elucidate the mechanism by which TG2 negatively regulates channel activity through covalent modification, we used a monoamine compound 5-biotinamido-pentylamine (BP) that contains both primary amine and biotin moieties. BP mimics a Lys residue, and TG2 can enzymaticaly incorporate BP into the Gln residue, which can be traced by horseradish peroxidase (HRP)-conjugated streptavidin. Therefore, we prepared BP-containing $IP_3R1$ using purified TG2 and P2/P3 vesicles (Fig. 2*B*). The IICR assay revealed that the BP-containing $IP_3R1$ has intact activity (Fig. 2*C*), indicating that the structures of both $IP_3$-binding and $Ca^{2+}$-permeating domains are not affected by the covalent incorporation of BP molecules. Removal of TG2 and BP followed by the addition of avidin proteins with a neutralized isoelectric point (NeutrAvidin) to the BP-containing $IP_3R1$ inhibited IICR in a dose-dependent manner (Fig. 2*D*). These results indicate that steric hindrance near the BP-containing Gln residue is important for the allosteric inhibition of IICR.

To examine the inhibitory role of endogenous TG2 in living cells, $Ca^{2+}$ imaging was performed using HeLa cells. TG2 silencing

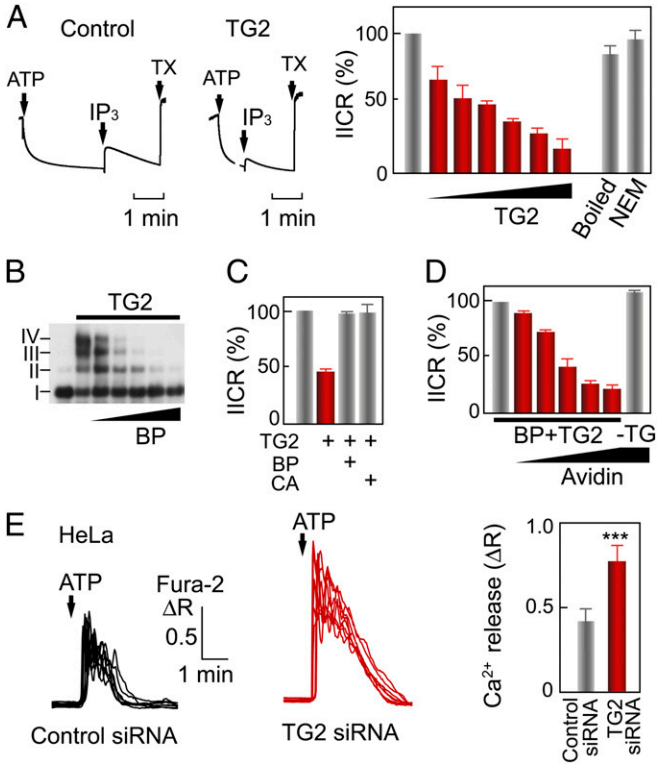


**Fig. 2.** TG2 inhibits $IP_3R1$-mediated $Ca^{2+}$ release. (*A*) Effects of purified TG2 on IICR from P2/P3 vesicles after $Ca^{2+}$ loading by adding 1 mM Mg–ATP. IICRs were evoked with 0.1 μM $IP_3$, and the total $Ca^{2+}$ pool was estimated using 10 mM Triton X-100 (TX). The bar graph summarizes the mean + SD from three independent experiments using P2/P3 vesicles pretreated with TG2 (0, 1, 2, 5, 10, 20, and 50 μg/mL), 10 μg/mL boiled TG2, or 10 μg/mL NEM–TG2. The $IC_{50}$ value of TG2 is 34 nM, calculated by a nonlinear regression analysis using a four-parameter logistic function. (*B*) The BP was incorporated into the $IP_3R1$ by TG2-catalyzed reactions. $IP_3R1$ was pretreated with both TG2 and BP (1, 2, 5, 10, and 20 mM), and the oligomeric status was confirmed using AGE. (*C*) The IICR from TG2-pretreated P2/P3 vesicles prepared in the presence of 10 mM BP or 10 mM cystamine (CA). (*D*) The BP-containing (BP + TG) or BP-lacking (–TG) P2/P3 vesicles were pretreated with 10 or 0 μg/mL TG2. The IICR was measured in the presence of 0, 31, 63, 94, 125, and 156 μg/mL (slope) or 156 μg/mL (–TG) of avidin. (*E*) Fura-2 ratio images of living HeLa cells transfected with control (black lines) or TG2 (red lines) siRNA for 48 h were obtained under a nominally $Ca^{2+}$-free condition. The bar graph represents the mean + SD of peak amplitudes (control siRNA, $n = 117$; TG2 siRNA, $n = 119$). ΔR indicates changes in the fura-2 ratio in response to 3 μM ATP. $***P = 8 \times 10^{-18}$.

significantly enhanced ATP-evoked $Ca^{2+}$ release in the $Ca^{2+}$-free condition (Fig. 2*E*), indicating that endogenous TG2 inhibits IICR activity in living cells.

**TG2 Negatively Regulates $IP_3R$-Mediated Autophagy.** Our data indicate that TG2 inhibits $IP_3R1$ function. To examine the physiological role of this regulation in the cellular functions of $IP_3R1$, we studied the role of TG2 and $IP_3R$ in autophagy. $IP_3R1$ regulates autophagy (24–27), and TG2 is also thought to regulate autophagy (50, 51); however, the interplay between TG2 and $IP_3R1$ in autophagy regulation has not been studied. We hypothesized that TG2 affects $IP_3R1$-mediated autophagy regulation. To examine autophagy, we used HeLa cells in which both $IP_3R1$ and TG2 were expressed dominantly. $IP_3R1$ knockdown increases LC3-II (lapidated microtubule-associated protein light chain 3, LC3, an index of autophagy) content without changing the amount of actin (Fig. 3*A*), consistent with previous reports (24–27). Furthermore, we found that TG2 knockdown had the opposite effect (Fig. 3*A*).

To clarify whether $IP_3R1$ mediated the TG2-dependent regulation of autophagy, we examined the $IP_3R1$ inhibitors xestospongin C (Xest) and 2-aminoethoxydiphenyl borate (2-APB). Xest and 2-APB block the TG2-dependent effect on autophagy (Fig. 3*A*) without affecting TG2 levels (Fig. S2*A*), suggesting that TG2 regulates autophagy through $IP_3R1$. To confirm this possibility in living cells, we observed the maturation of autophagosomes using a tandem fluorescent LC3 indicator containing both red (RFP) and green (GFP) fluorescent proteins (tfLC3) that distinguishes between autophagosomes and autolysosomes by quenching GFP fluorescence at lysosomal pH (52). In control siRNA-transfected cells, GFP and RFP puncta were independently distributed, indicating the presence of both autophagosomes and autolysosomes in the cells (Fig. 3*B*). However, $IP_3R1$ knockdown caused significant accumulation of autophagosomes that were colabeled with GFP and RFP fluorescence, whereas TG2 knockdown yielded predominantly RFP signals, as observed in amino acid deprivation (Fig. 3*B*). These results confirm that TG2 and $IP_3R1$ have opposing effects in the control of autophagy.

To verify the opposing effects of TG2 and $IP_3R1$ on autophagy, we monitored the dynamics of autophagosomes in living cells. Time-lapse imaging of tfLC3 revealed that the autophagosomes in control and TG2 siRNA-transfected cells actively moved inside cells, whereas the altered trafficking of autophagosomes was observed in $IP_3R1$ siRNA-transfected cells (Fig. S2*B*).

To confirm these observations, we monitored the distribution of endogenous autophagosomes and lysosomes in siRNA-transfected HeLa cells. In control and TG2–siRNA-transfected cells, LC3-labeled autophagosomes and lysosomal-associated membrane protein 1 (LAMP1)-labeled lysosomes were widely distributed in the cells and stochastically overlapped with each other (Fig. S2*C*). However, autophagosomes accumulated near the nucleus in cells transfected with $IP_3R1$ siRNA (Fig. S2*C*). These data confirmed the observations using tfLC3 indicators that autophagy was regulated by the opposing effects of TG2 and $IP_3R1$.

**The $IP_3R1$ Gln2746 Residue Is a Potent TG2 Substrate.** To elucidate the mechanism by which TG2 inhibited $IP_3R1$-mediated signaling, we performed limited digestion experiments to identify the site of TG2 modification in $IP_3R1$. Calpain digestion of $IP_3R1$ pretreated with TG2 revealed a marked decrease in the C-terminal 130-kDa (C130) and 85-kDa (C85) fragments but not the N-terminal 180-kDa (N180) or 100-kDa fragments (N100) (Fig. S3 *A* and *B*). Consistent with these observations, cross-linking by TG2 after limited digestion also resulted in a marked decrease in C130 recovery, whereas the amount of N180 was not altered by TG2 (Fig. S3*C*). These results indicate that cross-linking occurs between the C130 fragments but not the residual N180 fragments. To confirm this, we performed limited digestion of BP-containing $IP_3R1$ (Fig. S3 *D* and *E*). The apparent sizes of BP-labeled bands corresponded to the C130 and C85 fragments. Further digestion confirmed that the BP-labeled bands corresponded to the C-terminal fragment. Together, these results indicated that subunit cross-linking occurred within the C130 fragments.

To precisely determine the Gln (Q) donor site for $IP_3R1$ cross-linking, we performed mass spectrometric analyses. We pulled down endogenous substrates of TG2 from mouse brains by incorporation with BP. A band of ∼300 kDa was identified as mouse $IP_3R1$ by in-gel digestion and mass spectrometry (MS), indicating that $IP_3R1$ is a preferred substrate of TG2 (Fig. S4 *A* and *B*). Calculating the mass of BP, we found that the carboxyl-terminal peptide was exclusively modified among 63 Gln residues assigned by mass analysis (Fig. S4*C*). We determined the precise modified residue in $IP_3R1$ using liquid chromatography–MS (LC–MS), followed by tandem MS (MS/MS). This analysis identified one transamidation site of the Gln residue at position 2746 (Gln2746) (Fig. 4*A*). Compared with the wild-type peptide,

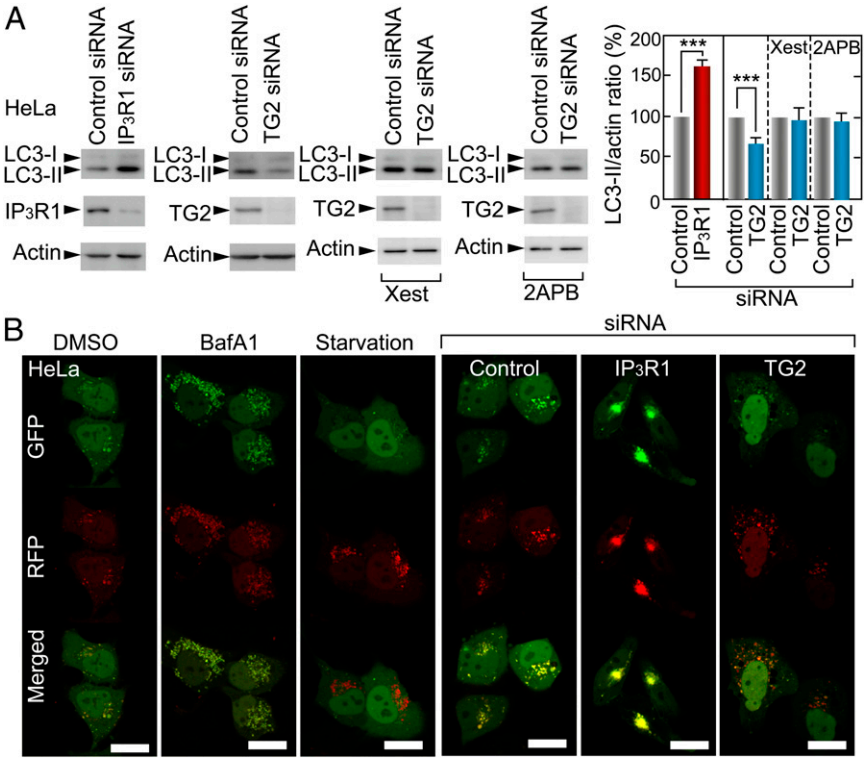


**Fig. 3.** TG2 negatively regulates $IP_3R1$-mediated autophagy processes. (*A*) LC3-I, LC3-II, $IP_3R1$, TG2, and actin levels in HeLa cells were evaluated 48 h after transfection with control, $IP_3R$, or TG2. We added 2 μM Xest or 100 μM 2-APB to HeLa cells 6 h after siRNA transfection. The bar chart represents the mean + SEM of LC3-II (LC3-II/actin ratio). ***$P$ = 0.0011 (control versus $IP_3R1$), ***$P$ = 0.0031 (control versus TG2). (*B*) Loss of $IP_3R1$ or TG2 affects autophagy as measured by GFP and RFP signals of an autophagosome indicator with tandem fluorophores (tfLC3) (52) in HeLa cells. We adjusted the sensitivity of microscopy for green and red signals using 10 nM BafA1- and amino-acid–deprived HeLa cells as negative and positive controls, respectively.

a clear mass shift corresponding to BP was detected in the modified peptide (Fig. 4*A*). The substrate specificity of TG2 was determined using the sequence motif QxPl (x, any; l, aliphatic amino acids) (53). The sequence containing Gln2746 is consistent with this motif, indicating that Gln2746, but not Gln2747, is a target of TG2. Peptides containing QxP motifs at Gln524, Gln1137, and Gln1219 in mouse $IP_3R1$ were detected by MS, but no BP incorporation was observed at these sites. Therefore, these Gln residues are not accessible to TG2 in the native conformation of tetrameric $IP_3R1$.

The QxP motif at Gln1705 might be modified by TG2 modification; therefore, we examined the cross-linking of mutants. We generated deletion mutants of the C-terminal domain of mouse $IP_3R1$ (calculated mass, 132.4 kDa, corresponding to the C130 fragment) and expressed them in COS-7 cells (Fig. 4*B*). We found that the recombinant wild-type (WT) channel was cross-linked by TG2, but the deletion mutant ΔQQPA (Fig. 4*C*) and the Q2746N mutant (Fig. 4*D*) were not cross-linked. These results indicate that the C-terminal QxP motif at Gln2746 was essential for subunit cross-linking. This motif is conserved among vertebrates including fish, birds, and mammals but not among invertebrates, suggesting that this regulation might be specific to vertebrates. The Gln2746-containing QxP motif is not conserved among other isoforms, but mouse $IP_3R2$ (Gln897, Gln1221, and Gln1997) and mouse $IP_3R3$ (Gln896, Gln1211, and Gln1948) also contain three QxP motifs. If these motifs are exposed and accessible to TG2, $IP_3R2/3$ might also be TG2 targets.

Next, we examined whether the Gln2746-containg motif is sufficient for cross-linking by TG2. The NPQQPA peptide, but not NPNQPA, reacted with tetramethylrhodamine cadaverine (TMR-cad) to produce a cross-linked product with TG2 (Fig. S4*D*). We confirmed the structure of this purified product using MS and subsequently subjected it to a de–cross-linking reaction with TG2. Incubation of the product with both TG2 and $CaCl_2$ formed a product that was consistent with TMR-cad (Fig. S4*E*). These data indicate that the Gln2746-containg motif is essential and sufficient for cross-linking by TG2.

Either isopeptide hydrolysis and/or deamidation by TG2 can generate a glutamate residue (E) at the position of the intrinsic Gln residue (Q) (34). To test this possibility, we generated the antibody αE2746, which specifically recognizes deamidated $IP_3R1$ (Fig. S5*A*). The site-specific αE2746 antibody detected TG2-catalyzed deamidation of tetrameric $IP_3R1$ in P2/P3 vesicles (Fig. S5*B*). The αE2746 antibody revealed the existence of deamidated $IP_3R1$ in cerebellar $IP_3R1$ (Fig. S5*C*), and LC–MS analysis also confirmed the deamidated $IP_3R1$ (Fig. S5 *D* and *E*). The specificity of the αE2746 antibody was further validated using the full-length $IP_3R1$ with Q2746E mutation (Fig. 5*A* and Fig. S5*F*).

**Modification of $IP_3R1$ in HD Models.** Our data indicated that the modification by TG2 impaired $IP_3R1$-mediated cellular processes; therefore, we hypothesized that this regulation might lead to cellular dysregulation under pathological conditions. TG2 is up-regulated in the brain in HD model mice, including R6/2 and YAC128 mice (54–57), and HD patients (49, 58–61). Therefore, we tested whether $IP_3R$ was modified by TG2 in these HD models.

We investigated TG2-mediated modification of $IP_3R1$ in an animal model of HD R6/2, which is transgenic (Tg) for exon 1 of the human Htt gene with 120 polyQ repeats, using the specific antibody that recognizes modified Gln2746 in $IP_3R1$ (Fig. 5*A*). The brain P2/P3 vesicles were obtained from the cerebrum including the striatum and the cortex or the cerebellum (CB) of three litter pairs of 4-wk-old and 12-wk-old HD model mice (R6/2 Tg or WT); we observed endogenous $IP_3R1$ using αE2746 and

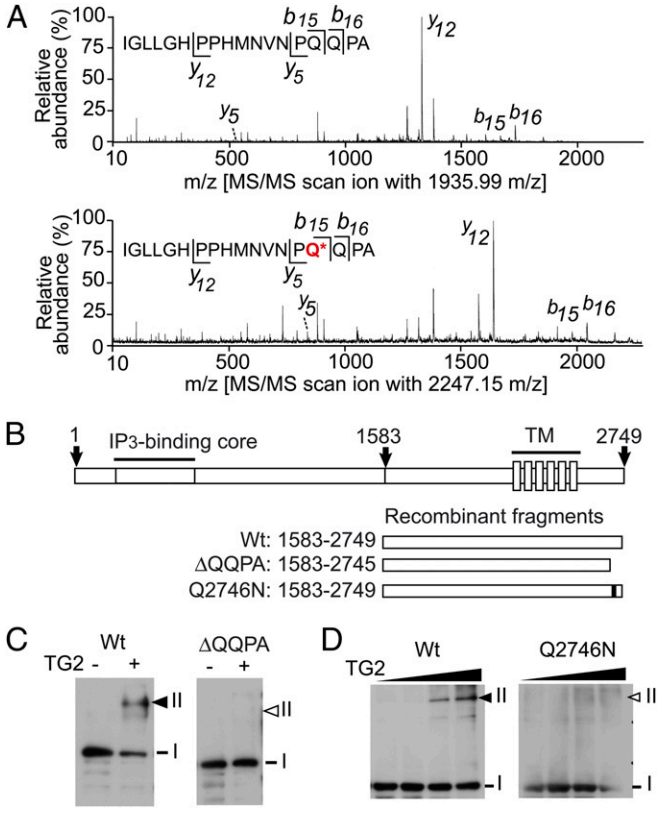


**Fig. 4.** Gln2746 of $IP_3R1$ is modified by TG2. (*A*) $IP_3R1$ was modified at Gln2746 by TG2. MS/MS scanned the C-terminal peptide of $IP_3R1$ with ion *m/z* 1,935.99 (*Upper*) and the biotinylated peptide with *m/z* 2,247.15 (*Lower*). The *b* and *y* ions are indicated on the MS/MS spectra. The asterisk denotes a modified Gln residue (see also Fig. S4). (*B*) A scheme shows the primary structure of $IP_3R1$ and recombinant proteins corresponding to C-terminal 130-kDa fragments generated by calpain cleavage (Fig. S3). WT, a mutant in which four C-terminal amino acids were deleted (ΔQQPA), and a point mutant containing a Gln2746 to Asn substitution (Q2746N) are shown in the scheme. (*C*) The lower gels show intersubunit cross-linking of WT and ΔQQPA expressed in COS-7 cells. (*D*) Intersubunit cross-linking of WT and Q2746N expressed in COS-7 cells. Black and white arrows indicate the cross-linked dimer and its corresponding size, respectively.

4C11 that detects both modified and unmodified $IP_3R1$. The $IP_3R1$ expression levels were suppressed particularly in 12-wk-old HD mice (16, 28); thus, we normalized the αE2746 signal to the 4C11 signal. The relative level of the αE2746 signal was significantly higher in the brains of both 4-wk-old and 12-wk-old R6/2 Tg mice compared with WT mice (Fig. 5*B*).

TG2 up-regulation has been observed in the brain and lymphocytes of patients with HD (49, 58–61); therefore, we examined a role of TG on $IP_3R$ activity in B-lymphocytes from HD patients. Pretreatment with a specific TG blocker (Z-DON–Val–Pro–Leu–OMe, ZDON) (56, 62) enhanced $IP_3R$-mediated $Ca^{2+}$ release during B-cell antigen receptor stimulation by the anti-IgM antibody, which evoked IICR (63) in lymphocytes from a patient with HD (Fig. 5*C*). Notably, this effect was consistently observed in three individuals with HD. This indicates that in addition to the modification in the structure of $IP_3R$ in HD model mice (Fig. 5*B*), TG modifies the function of $IP_3R$ in B-lymphocytes from HD patients (Fig. 5*C*).

We observed the effects of the human Htt mutant on $Ca^{2+}$ signaling in other HD models. The induced expression of the full-length human Htt including 145 polyQ in PC12 cells impaired acetylcholine (ACh)-evoked $Ca^{2+}$ release under $Ca^{2+}$-free conditions, whereas the enhanced ACh-evoked $Ca^{2+}$ increase (Fig. S6*A*) was observed in the presence of extracellular $Ca^{2+}$ in line with the sensitized $Ca^{2+}$ increase in YAC128 neurons (64–66). To verify the inhibitory effect of the Htt mutant, we observed $Ca^{2+}$ release in Neuro2a cells transiently expressing the myc-tagged full-length Htt including 23 polyQ (Htt23Q–myc) or 145 polyQ (Htt145Q–myc). The $Ca^{2+}$ release upon stimulation by bradykinin (BK) in Neuro2a cells expressing with Htt145Q–myc was less than Htt23Q–myc under $Ca^{2+}$-free conditions (Fig. S6*B*). Transient expression of Htt exon1 including 60 polyQ (eHtt60Q–EGFP) or 150 polyQ (eHtt150Q–EGFP) also impaired $Ca^{2+}$ release in Neuro2a cells compared with the control (eHtt18Q–EGFP) (Fig. S6*C*), and the 3,5-dihydroxy phenylglycine (DHPG)-evoked $Ca^{2+}$ increase in eHtt150Q–EGFP-expressing neurons was lower compared with eHtt18Q–EGFP-expressing neurons (Fig. S6*D*). To examine the involvement of TG2-dependent modification, we transfected Neuro2a cells coexpressing eHtt150Q–EGFP with either a Gln2746 mutant fragment (AQPA) or a Gln2746-containing fragment (QQPA). Overexpression of QQPA enhanced $Ca^{2+}$ release compared with AQPA (Fig. S6*D*), suggesting the involvement of TG2-dependent modification. We also examined the Gln2746 modification in Neuro2a cells inducibly expressing Htt exon1 including 16 polyQ (eHtt16Q–EGFP) or 150 polyQ (eHtt150Q–EGFP) using the αE2746 antibody. Western blotting of endogenous $IP_3R1$ (Fig. 6*E*) and immunostaining of the overexpressed $IP_3R1$ C terminus (Fig. 6*F*) demonstrate that the αE2746-detectable modification was enhanced in the Neuro2 cells with eHtt150Q–EGFP after 48-h induction compared to those with eHtt16Q–EGFP.

## Discussion

The role of defective allostery in ER-resident calcium channels in subsequent cellular defects in neurological disorders remains unclear. The current study addresses this issue, demonstrating a novel allosteric mechanism—the covalent modification of $IP_3R$ structure and function—as well as its implications for the etiology of neurological diseases. Specifically, we discovered that TG2 in the brain regulates $IP_3R1$ by catalyzing a posttranslational modification at the Gln side chain of the Gln2746 residue. Up-regulation of TG2 enhanced the Gln modification of $IP_3R1$, and TG2 suppressed $IP_3R1$-mediated $Ca^{2+}$ signaling and subsequent cellular processes. Modification of Gln2746 and $IP_3R1$ function was observed in HD models and B-lymphocytes from HD patients; these results therefore suggest a novel mechanism linking the activation of brain TG to the control of $IP_3R$-mediated $Ca^{2+}$ signaling in HD. Based on these results, we propose a general model for the progressive brain dysfunction observed in brain pathogenesis that involves aberrant $IP_3R$ signaling.

An important point in this study is the identification of TG2 as a chronic regulator of $IP_3R1$ structure and function. This finding has broad implications for pathological neuronal function and degeneration because it links TG2 functions in cellular differentiation, cellular stress, and inflammation (34, 35) to the chronic defects in $Ca^{2+}$ signaling. Numerous literatures have demonstrated that TG2 is up-regulated in various diseases including HD (49, 54, 55, 59–61), AD (37, 38, 40, 42, 43, 45), and PD (39, 44). The splicing mechanism (67, 68) and stress-dependent inductions (34, 35, 69–72) are considered to elucidate the up-regulation, and the increased $Ca^{2+}$ levels observed in many diseases (4, 17–22) are also competent to trigger TG2 activation. The $Ca^{2+}$-dependent activation of TG2 inhibits the $IP_3R1$-mediated $Ca^{2+}$ release, as revealed in the current study; thus, this enzymatically allosteric modulation should primarily contribute to a negative feedback mechanism to maintain homeostatic control of intracellular $Ca^{2+}$ levels. However, this modification subsequently would have a chronically negative effect on $Ca^{2+}$ signaling, because it is much more static than noncovalent allosteric modulators required for the control of rapid and dynamic $Ca^{2+}$ signaling such as $Ca^{2+}$ oscillation. Therefore, the TG2-dependent allosteric modulation should chronically set in motion cascades of defective signaling

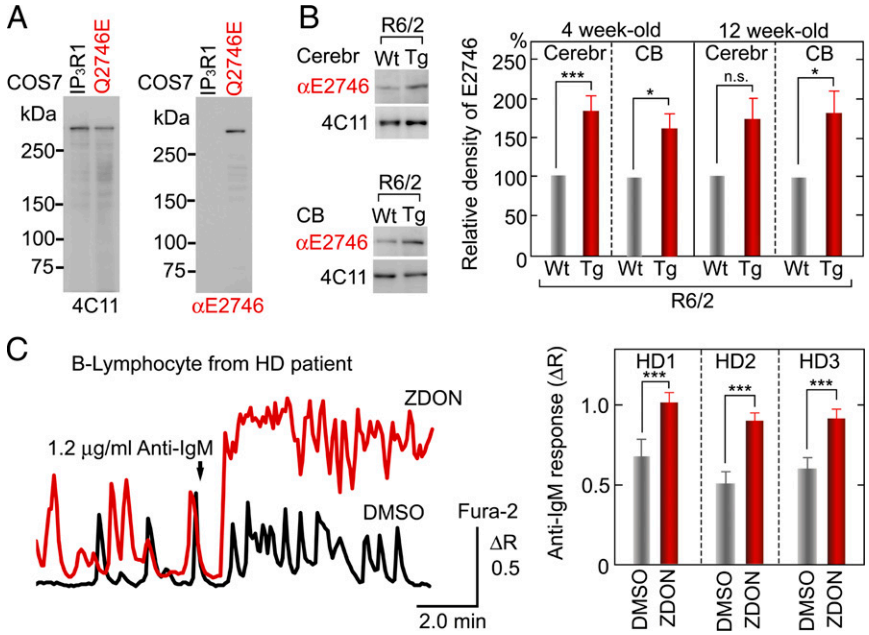


**Fig. 5.** $IP_3R1$ structure and function are modified in HD models. (*A*) The 4C11 monoclonal antibody (*Left*) detected both full-length $IP_3R1$ and Q2746E mutant expressed in COS-7 cells, whereas our newly developed αE2746 antibody (*Right*) detected only the Q2746E mutant. (*B*) Gln2746 modification in endogenous $IP_3R1$ in HD models. Blotted endogenous $IP_3R1$ in mouse P2/P3 fractions was prepared from the cerebrum (cerebr) containing the cortex and the striatum (*Upper*) or the CB (*Lower*) of 4-wk-old WT or Tg male R6/2 mice. The loading volumes were adjusted based on the total $IP_3R1$ content. The bar charts represent the mean + SEM of normalized Gln2746 modification in three-litter pairs of 4-wk-old and 12-wk-old R6/2 mice. Relative amounts of Gln2746 modification were calculated from the ratio of the αE2746 signal to the 4C11 signal. Four weeks, $*P = 0.025$, $***P = 0.0099$; 12 wk, $P = 0.051$ (not significant, n.s), $*P = 0.049$. (*C*) Rescue of $Ca^{2+}$ signaling in HD patient cells by inhibition of TG2. Black and red lines show $IP_3R$-mediated $Ca^{2+}$ release by anti-IgM (1.2 μg/mL) stimulation in B-lymphocytes obtained from an HD patient (HD1). Bar charts represent the mean + SEM of peak amplitudes of anti–IgM-induced $Ca^{2+}$ release in lymphocytes from three HD patients [HD1, $***P = 0.0078$ (control, $n = 21$; ZDON, $n = 38$); HD2, $***P = 7.3 \times 10^{-5}$ (control, $n = 34$; ZDON, $n = 54$); HD3, $***P = 5.9 \times 10^{-5}$ (control, $n = 15$; ZDON, $n = 48$)] pretreated with DMSO (control) or a site-directed TG inhibitory peptide ZDON (100 μM) for 30 min. HD1, HD2, and HD3 correspond to GM5560, GM6773, and GM4830, respectively. The peak amplitude was calculated as the difference between the mean value before stimulation and the peak value during stimulation.

related to pathological states; up-regulation of TG2 may disrupt the $IP_3R1$-mediated plasticity of neuronal signaling (3, 10–12) and the homeostatic control of cellular processes including mitochondria energy production (23), autophagy regulation (24–27), ER stress (28), and others (29–31) and ultimately increases cellular stress, resulting in further TG2 up-regulation proceeding a vicious cycle. Given the widespread brain expression profiles of TG2 and $IP_3R1$, we propose that the mechanism described in this study might potentially serve as a general principle for many other diseases of the brain or other tissues in which TG2 is up-regulated by a disease-initiating agent. In this study, we assume that the disease-initiating agent is the mutant Htt; future studies are required to examine whether other disease-initiating agents such amyloid proteins in AD and α-synuclein in PD also would cause chronic TG2 activation, resulting in $IP_3R$ modification and aberrant calcium signaling, and suggesting its presumable role in brain dysfunctions including cognitive declines occurs frequently during the prodromal states of these neurodegenerative diseases (73–77).

This study revealed that the covalent modification by TG2 results in three alternative states, as shown in Fig. 6; thus, the other roles of TG2 in $Ca^{2+}$ signaling are also conceivable. TG2 inhibits IICR activity by both cross-linking and steric hindrance around Gln2746 (Fig. 2), whereas functional analysis of Q2746E indicates that deamidation of $IP_3R1$ suppresses TG2-mediated inhibition (Fig. S6*G*). All potential modifications are shown in the schematic diagram, but the overall activity of a single channel would depend significantly on the relative number of cross-linked isopeptide bonds, amine incorporations, and deamidation in the tetramer. Acute increases in $Ca^{2+}$ levels cause subunit cross-linking in neuroblastoma and glioblastoma cells (Fig. 1*E*), whereas amine incorporation and deamidation were observed in resting cells and brain tissues without stimulation by increasing $Ca^{2+}$ concentrations (Fig. 5*B* and Figs. S5 *C–E* and S6 *H* and *I*). The deamidation reaction by TG2 is dependent on pH (78) and substrate affinity (79); therefore, the relative abundance of these three modifications is presumably determined by the cellular state and the conformation around Gln2746. These irreversible processes would contribute to chronic changes in homeostasis of $Ca^{2+}$ signaling and subsequent cellular processes, whereas the TG2-resistant states including the small amine-containing $IP_3R1$, such as BP incorporation shown in Fig. 2*C* and/or the deamidated $IP_3R1$ shown in Fig. S6*G*, might contribute to $Ca^{2+}$-dependent cell death, including apoptosis (2, 17), due to the lack of negative feedback regulation by $Ca^{2+}$. Although deletion of the C-terminal 12 amino acids has no effect on IICR (80), binding of the specific monoclonal antibody 18A10 (81) and GIT1 to this region inhibits IICR (82), similar to the BP–avidin complex in this study. Because both IgG and GIT1 form bulky architectures, these observations are consistent with our conclusion that large molecules such as avidin but not small moieties such as BP interfere with configuration changes by steric hindrance. IICR is regulated by binding of the C-terminal region near Gln2746 by various proteins governing cellular fate—for example, Bcl-$X_L$, Bcl-2, cytochrome *c*, HAP1, and Htt (4, 5, 17, 18); thus, we speculate that the $IP_3R1$ C terminus might act as a signaling hub whose structure affects cellular processes by regulating the subunit configuration by steric hindrance. Considering the direct activation of $IP_3R1$ by the Htt mutant (18), the net activity of $IP_3R1$ may be comprehensively determined by the Htt mutant and TG2 in HD. The impairment of $Ca^{2+}$ release by eHtt150Q–EGFP

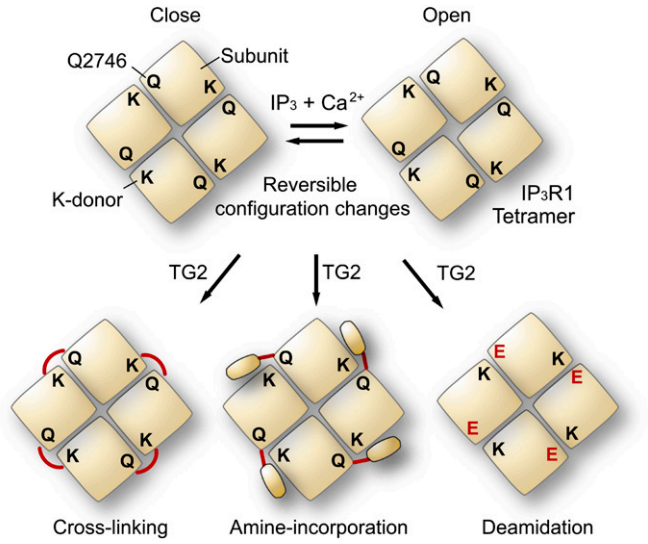


**Fig. 6.** Model for TG2-mediated regulation of $IP_3R1$. Schematic diagrams indicating the subunit arrangement of the allosteric coupling domain within the C-terminal 130-kDa region (C130) of $IP_3R1$. The Q-donor at the C terminus is located in close proximity to the K-donor region of the neighboring subunit. We propose reversible configuration changes between the closed and open states in tetrameric $IP_3R1$. TG-catalyzed transamidation causes covalent intersubunit cross-linking, which locks the closed configuration. A large molecule such as avidin but not a small moiety such as BP inhibits the motion by amine incorporation. Gln2746 of $IP_3R1$ is deamidated by TG2 and converted into a glutamate residue that is resistant to TG2-mediated inhibition.

was more potent than Htt145Q–myc (Fig. S6 *B* and *C*), consistent with higher TG2 activities in R6/2 than YAC128 mice expressing the full-length Htt mutant (55, 57) and the sensitized $Ca^{2+}$ increase in YAC128 mice more than shortstop mice expressing Htt exon1/2 (64). The poly-Gln repeat of the Htt mutant is a favorable substrate of TG2 (41); thus, the possibility of substrate competition and steric hindrance around Gln2746 is also interesting. Thereby, we suggest that the prevalence of full-length Htt mutant and TG2 modulations on $IP_3R1$ may determine the total net activity of $Ca^{2+}$ signaling from the ER and the pathological states in HD—that is, the prodromal decline of neural signaling or the degeneration by apoptosis.

The first insight into the mechanism underlying the coupling between the IBD and the channel domain by $IP_3$-evoked structural changes was described more than two decades ago (83). From our early EM studies of negatively stained $IP_3R1$ using heparin-gold labeling, we proposed a long-range coupling of IBD to the channel domain by $Ca^{2+}$-dependent structural changes (84–86). However, direct binding of the IBD to the channel domain was postulated, and a model was proposed in which an N-terminal suppressor domain directly binds a loop between putative transmembrane helices (87–90). Recently, highly improved cryo-EM reconstruction was reported (9), and by fitting calculations using X-ray structures (7, 8), it was concluded that direct interaction of the IBD with the channel domain is unlikely (8). However, because the X-ray structure of the IBD is limited to only 5% of each tetramer, which is equivalent to 20% of each subunit, the role of the other domains in channel gating remains unclear (91). Here, we show new evidence demonstrating that configuration changes outside the IBD are required for channel activation (Fig. 6). Our data are consistent with the conclusion that the Gln2746 in the C-terminal tail is proximal to the neighboring $IP_3R1$ subunit, and TG2 covalently tethers Gln2746 to the adjacent subunit by the Gln–Lys isopeptide bond that locks the channel in a closed configuration (Fig. 6). Notably, our BP incorporation experiments indicate that the isopeptide bond occurs outside the IBDs without impairing the intrinsic structures required for $IP_3$ binding and $Ca^{2+}$ permeation (Fig. 2 *B–D*). $IP_3R1$ function was not inhibited by transamidation of a small molecule such as BP; however, the subsequent addition of a bulky molecule such as avidin completely blocked receptor function (Fig. 2 *B–D*), indicating that steric hindrance near Gln2746 is crucial. We propose that an "allosteric coupling domain" in the C-terminal 130-kDa region (C130) exists between the IBD and the transmembrane domains to couple the IBD to the channel and that configuration changes in this domain are required for channel activation (Fig. 6). The *Eco*RI fragment-encoded short domain (ES; amino acids 2216–2749) of $IP_3R1$ is sufficient for tetramer formation (92), but the channel in the ES tetramer is always open (93). Therefore, the allosteric coupling domain presumably keeps the channel closed, and the transition to the open configurations could revert to the default channel state that constitutively permeates $Ca^{2+}$—for instance, the leaky channel assembled from ES domains.

What is the key mechanism regulating the allosteric transitions during channel activation? Two intrinsic determinants stabilizing the subunit configurations can be considered a priori—$IP_3$ and $Ca^{2+}$—because channel activation requires both $IP_3$ and $Ca^{2+}$. In fact, the recent X-ray structures of the IBD indicate that conformational changes occur upon $IP_3$ binding (7, 8); our group and others have demonstrated $Ca^{2+}$-induced structural changes (84, 85, 94, 95). Fluorescence resonance energy transfer (FRET) analysis of recombinant $IP_3Rs$ also showed reversible structural changes induced by physiological concentrations of $IP_3$ and $Ca^{2+}$ (96). Considering these observations and our current data, we propose that structural changes by $IP_3$ and $Ca^{2+}$ determine the configuration of the allosteric coupling domain. Given the $Ca^{2+}$-sensor site at E2100 (32) and the deletion site in *opisthotonos* mice (33) are located in this domain, these allosteric sites presumably control subunit configurations within this domain. These ligands—that is, $IP_3$, $Ca^{2+}$, and ATP—might confer a predominantly open configuration by noncovalent binding, but the covalent Gln–Lys isopeptide bonds and steric hindrance around Gln2746 are more energetically stable; therefore, these modifications can robustly and chronically lock the closed subunit configuration.

In summary, we identified TG2 as an $IP_3R1$-modifying enzyme that irreversibly controls the essential function of $IP_3R1$ in $Ca^{2+}$-signaling and subsequent cellular processes whose homeostasis is crucial for cellular fate and uncovered the allosteric mechanism by which $IP_3R$ channel activation is controlled by ligand binding. Many functional proteins undergo allosteric regulation; therefore, understanding allosteric mechanisms can elucidate the mechanisms underlying functions of these proteins and pave the way for drug design (1). This is the first demonstration, to our knowledge, of $IP_3R1$ allosteric transitions locked by TG2-catalyzed cross-linking, and these observations might provide a new framework for TG2-dependent enzymatic regulation of ligand-gated ion channels and allosteric proteins similar to $IP_3R1$.

## Materials and Methods

**Cell Culture.** SH-SY5Y, U87-MG, HeLa, and COS-7 cells were cultured in DMEM containing 10% (vol/vol) heat-inactivated FBS, 50 U/mL penicillin, and 50 μg/mL streptomycin. Human B-lymphocytes from patients with HD were obtained from the Coriell Institute (GM5560, GM6773, and GM4830) and cultured in RPMI medium 1640 containing 10% (vol/vol) heat-inactivated FBS, 50 U/mL penicillin, and 50 μg/mL streptomycin. All cells were maintained in 5% (vol/vol) $CO_2$ at 37 °C. The differentiation medium supplemented with 20 μM RA was replaced every 48 h for the SH-SY5Y and U87-MG cells. All of the animals were ethically treated according to the guidelines of the Animal Experiments Committee of the Institute of Physical and Chemical Research (RIKEN) Brain Science Institute.

**Transfection of siRNAs or Plasmids.** The siRNAs and human negative controls were purchased from B-Bridge. The nucleotide sequence of the TG2 siRNA was ggucaaugccgacguggua. $IP_3R1$ knockdown was performed as described previously

(28). The siRNA and ptfLC3 were transfected in HeLa cells using Lipofectamine 2000 (Invitrogen) and TransIT (Mirus) transfection reagents, respectively.

**Preparation of P2/P3 Fractions.** Mouse brains were washed extensively with chilled PBS and were then homogenized in a homogenate buffer (pH 7.5) composed of 10 mM 4-(2-hydroxyethyl)-1-piperazineethanesulfonic acid (Hepes)/sodium hydroxide (NaOH), 0.32 M sucrose, 1 mM ethylene diamine tetraacetic acid (EDTA), 2 mM Tris(2-carboxyethyl)phosphine (TCEP), and protease inhibitors (0.2 mM phenylmethylsulfonyl fluoride, 10 μM leupeptin, 10 μM pepstatin A, and 10 μM E-64). The homogenates were centrifuged at 800 × *g* for 5 min at 4 °C, and the resultant supernatants were subjected to ultracentrifugation at 105,000 × *g* for 60 min at 2–4 °C as previously described (97). The precipitates were suspended in resuspension buffer ResB (pH 7.5), containing 50 mM Hepes–NaOH, 150 mM NaCl, 1 mM EDTA, 2 mM TCEP, and protease inhibitors. The supernatant obtained after ultracentrifugation was used as the cytosolic fraction. The protein concentrations in the solution were estimated, adjusted to 3 mg/mL using ResB, and the samples were then quickly frozen in liquid nitrogen for storage until use in various experiments.

**Analysis of Intersubunit Cross-Linking Within $IP_3R1$ by Electrophoresis.** We estimated the cross-linking between $IP_3R1$ subunits using 1% AGE. The samples containing mouse cerebellar P2/P3 proteins (0.75–2.25 μg) were loaded in individual wells. Agarose was dissolved in a buffer containing 0.1% SDS using a microwave device. The agarose was heated and then gently mixed by manual rotation. The 1% agarose solution was poured into an acrylic tray (Nihon Eido) in which a 26-lane comb was placed. After 30 min at room temperature, the apparatus was filled with the electrolyte buffer, and the comb was carefully removed. Electrophoresis was performed at 100 V for 1–2 h. Immediately following electrophoresis, the agarose gels were placed in transfer buffer for 30 min. The separated proteins were transferred to a polyvinylidene difluoride (PVDF) membrane (Millipore). $IP_3R1$ was detected using the 4C11 monoclonal antibody as described previously (28, 97). A molecular marker was prepared by cross-linking bovine thyroglobulin with 1 mM 1,8-bis-maleimido-diethyleneglycol overnight at 4 °C.

**Measurement of $Ca^{2+}$ Release Activity of $IP_3R1$.** We loaded fura-2AM (Dojindo) into HeLa cells and B-lymphocytes by incubation with 5 μM fura-2AM in balanced salt solution (pH 7.4) containing 115 mM NaCl, 5.4 mM KCl, 2 mM $CaCl_2$, 1 mM $MgCl_2$, 20 mM Hepes, and 10 mM glucose for 30 min at room temperature, and performed $Ca^{2+}$ imaging using inverted fluorescence microscopy with a 20× objective lens (S Fluor 20× N.A. 0.75) (Nikon) and AQUACOSMOS (Hamamatsu Photonics) to obtain F340/F380 ratio images as described previously (28, 98). For measurements of IICR, the P2/P3 membranes (3 mg/mL protein) of mouse cerebella were washed three times with a buffer (pH 7.4) containing 50 mM Hepes–KOH, 110 mM KCl, 10 mM NaCl, and 5 mM $KH_2PO_4$. The washed 10-μL P2/P3 membranes (2 mg/mL protein) of the cerebella were added to 287 μL of a buffer containing 1 mM 2-mercaptoethanol, 1 μM $CaCl_2$, and 0.2 μM fura-2 in a cuvette. To introduce $Ca^{2+}$ into P2/P3 membrane vesicles, we added 3 μL of 100 mM Mg–ATP to the cuvette with stirring. Ratiometric measurement of fura-2 was performed at 30 °C using a CAF-110 (Jasco) or an F-2500 spectrofluorometer (Hitachi).

**Analysis of Autophagosome Dynamics by Fluorescence Microscopy.** We used ptfLC3 plasmids (52) expressing mRFP–GFP–LC3 to monitor autophagic processes in living cells. Cells plated in a 35-mm glass-bottomed dish were transfected with siRNA in Lipofectamine 2000 transfection reagent (Invitrogen) and then with 1 μg ptfLC3 by TransIT transfection reagent (Mirus) 6 h after the siRNA transfection. We observed GFP and RFP fluorescence signals in living cells under an FV1000D confocal microscope (Olympus) with a stage top incubator in 5% $CO_2$ at 37 °C.

**Affinity Purification of TG2 Substrates.** We incubated the reaction solution containing the P2/P3 fractions (1 mg/mL protein), 50 mM Hepes–NaOH (pH 7.5), 150 mM NaCl, 10 mM BP, 1 mM EGTA, 2 mM $CaCl_2$, and 30 ng/mL TG for 30 min at 37 °C. The mixture was centrifuged at 20,000 × *g* for 30 min at 4 °C, and the pellets were washed with 50 mM Hepes–NaOH (pH 7.5). The proteins were solubilized with 1% (wt/vol) 3-[(3-cholamidopropyl)dimethylammonio]-1-propanesulfonate (CHAPS) and mixed with avidin–agarose. After washing three times with the 1% CHAPS-containing Hepes buffer, the biotin-containing proteins bound to avidin–agarose were subjected to SDS/PAGE and were detected by Coomassie brilliant blue (CBB) staining or Western blotting analysis. The CBB-stained band was excised, digested using an in-gel digestion protocol, and analyzed by MS using MALDI-TOF MS (ABI).

**Specific Antibody Against Modified $IP_3R1$.** To examine the status of Gln2746 in mouse $IP_3R1$, a deamidated peptide (PPHMNVNPEQPA) corresponding to amino acids 2738–2749 was synthesized and conjugated to keyhole limpet hemocyanin via a cysteine added to the N terminus of the peptide. Japanese white rabbits were immunized with these peptides. The resulting polyclonal antibody was first applied to an affinity resin immobilized with a control peptide (PPHMNVNPQQPA) via cysteine added to the amino terminus, and the flow-through was applied onto a resin immobilized with the deamidated peptides. The specific antibody against the deamidated peptide was eluted with 100 mM glycine–HCl buffer (pH 2.5). To verify the specificity of the antibodies, we prepared recombinant $IP_3R1$, which was expressed as an EGFP–fusion protein (28). The PCR product was inserted into EGFP–$IP_3R1$-containing pcDNA3.1 vector with EcoRI and XhoI. Mutation of the Gln residue at the amino acid position of 2746 was confirmed by sequence analysis using an ABI 3730xl automatic sequencer. To confirm the specificity of the E2746 antibody, the C-terminal fragment of $IP_3R1$ (66 amino acids) was subcloned into the bacterial expression vector pGEX-6p (GE Healthcare) using EcoRI and SalI. Quantification of modified or native $IP_3R1$ was performed by densitometric analysis of Western blots using Image J software (National Institute of Health).

**Statistical Analysis.** All probability calculations were performed using unpaired and two-tailed Student *t* tests. The significance after multiple comparisons was estimated by the Bonferroni method or by Dunnett's method. For all data, no statistics were used for predetermination of the sample size, randomization, or blinding.

**ACKNOWLEDGMENTS.** We are grateful to Dr. T. Yoshimori (Osaka University) for the ptfLC3 plasmid and Dr. C. Yokoyama (RIKEN) for constructive comments on our manuscript. We thank the RIKEN Research Resources Center (RRC) for common-use equipment, M. Usui and K. Otsuki (RIKEN RRC) for assistance with MS, the RIKEN Brain Science Institute (BSI)–Olympus Collaboration Center for technical support, as well as M. Kurosawa, H. Miyazaki, and T. Yamanaka (RIKEN) for the HD model mice, cells, and plasmids. We are grateful to Y. Shimizu (Japan Science and Technology Agency, JST) for JST office management. This study was supported by JST International Cooperative Research Project–Solution Oriented Research for Science and Technology (K.M.); Japan Society for the Promotion of Science Grants-in-Aid for Scientific Research S [25221002 (to K.M.)], Scientific Research C [24500451 (to C.H.)], and Encouragement of Scientists [24926012 (to A.T.)]; and RIKEN BSI Grant and President's Fund (to K.M.).

1. Changeux JP (2013) 50 years of allosteric interactions: The twists and turns of the models. *Nat Rev Mol Cell Biol* 14(12):819–829.
2. Berridge MJ, Lipp P, Bootman MD (2000) The versatility and universality of calcium signalling. *Nat Rev Mol Cell Biol* 1(1):11–21.
3. Mikoshiba K (2007) IP3 receptor/Ca2+ channel: From discovery to new signaling concepts. *J Neurochem* 102(5):1426–1446.
4. Foskett JK, White C, Cheung KH, Mak DO (2007) Inositol trisphosphate receptor Ca2+ release channels. *Physiol Rev* 87(2):593–658.
5. Patterson RL, Boehning D, Snyder SH (2004) Inositol 1,4,5-trisphosphate receptors as signal integrators. *Annu Rev Biochem* 73:437–465.
6. Furuichi T, et al. (1989) Primary structure and functional expression of the inositol 1,4,5-trisphosphate-binding protein P400. *Nature* 342(6245):32–38.
7. Lin CC, Baek K, Lu Z (2011) Apo and $InsP_3$-bound crystal structures of the ligand-binding domain of an $InsP_3$ receptor. *Nat Struct Mol Biol* 18(10):1172–1174.
8. Seo MD, et al. (2012) Structural and functional conservation of key domains in InsP3 and ryanodine receptors. *Nature* 483(7387):108–112.
9. Ludtke SJ, et al. (2011) Flexible architecture of IP3R1 by Cryo-EM. *Structure* 19(8): 1192–1199.
10. Nishiyama M, Hong K, Mikoshiba K, Poo MM, Kato K (2000) Calcium stores regulate the polarity and input specificity of synaptic modification. *Nature* 408(6812): 584–588.
11. Harnett MT, Bernier BE, Ahn KC, Morikawa H (2009) Burst-timing-dependent plasticity of NMDA receptor-mediated transmission in midbrain dopamine neurons. *Neuron* 62(6):826–838.
12. Sugawara T, et al. (2013) Type 1 inositol trisphosphate receptor regulates cerebellar circuits by maintaining the spine morphology of purkinje cells in adult mice. *J Neurosci* 33(30):12186–12196.
13. Di Gregorio E, et al. (2010) Two Italian families with ITPR1 gene deletion presenting a broader phenotype of SCA15. *Cerebellum* 9(1):115–123.
14. Hara K, et al. (2008) Total deletion and a missense mutation of ITPR1 in Japanese SCA15 families. *Neurology* 71(8):547–551.
15. Yamazaki H, et al. (2011) Functional characterization of the P1059L mutation in the inositol 1,4,5-trisphosphate receptor type 1 identified in a Japanese SCA15 family. *Biochem Biophys Res Commun* 410(4):754–758.
16. Luthi-Carter R, et al. (2000) Decreased expression of striatal signaling genes in a mouse model of Huntington's disease. *Hum Mol Genet* 9(9):1259–1271.

17. Bezprozvanny I (2009) Calcium signaling and neurodegenerative diseases. *Trends Mol Med* 15(3):89–100.
18. Tang TS, et al. (2003) Huntingtin and huntingtin-associated protein 1 influence neuronal calcium signaling mediated by inositol-(1,4,5) triphosphate receptor type 1. *Neuron* 39(2):227–239.
19. Cheung KH, et al. (2008) Mechanism of Ca2+ disruption in Alzheimer's disease by presenilin regulation of InsP3 receptor channel gating. *Neuron* 58(6):871–883.
20. Popugaeva E, Bezprozvanny I (2013) Role of endoplasmic reticulum Ca2+ signaling in the pathogenesis of Alzheimer disease. *Front Mol Neurosci* 6:29.
21. Mattson MP (2004) Pathways towards and away from Alzheimer's disease. *Nature* 430(7000):631–639.
22. Shilling D, et al. (2014) Suppression of InsP3 receptor-mediated Ca2+ signaling alleviates mutant presenilin-linked familial Alzheimer's disease pathogenesis. *J Neurosci* 34(20):6910–6923.
23. White C, et al. (2005) The endoplasmic reticulum gateway to apoptosis by Bcl-X(L) modulation of the InsP3R. *Nat Cell Biol* 7(10):1021–1028.
24. Cárdenas C, et al. (2010) Essential regulation of cell bioenergetics by constitutive InsP3 receptor Ca2+ transfer to mitochondria. *Cell* 142(2):270–283.
25. Decuypere JP, et al. (2011) Ins(1,4,5)P3 receptor-mediated Ca2+ signaling and autophagy induction are interrelated. *Autophagy* 7(12):1472–1489.
26. Vicencio JM, et al. (2009) The inositol 1,4,5-trisphosphate receptor regulates autophagy through its interaction with Beclin 1. *Cell Death Differ* 16(7):1006–1017.
27. Criollo A, et al. (2007) Regulation of autophagy by the inositol trisphosphate receptor. *Cell Death Differ* 14(5):1029–1039.
28. Higo T, et al. (2010) Mechanism of ER stress-induced brain damage by IP(3) receptor. *Neuron* 68(5):865–878.
29. Wang Y, et al. (2012) Inositol-1,4,5-trisphosphate receptor regulates hepatic gluconeogenesis in fasting and diabetes. *Nature* 485(7396):128–132.
30. Futatsugi A, et al. (2005) IP3 receptor types 2 and 3 mediate exocrine secretion underlying energy metabolism. *Science* 309(5744):2232–2234.
31. Lee GS, et al. (2012) The calcium-sensing receptor regulates the NLRP3 inflammasome through Ca2+ and cAMP. *Nature* 492(7427):123–127.
32. Miyakawa T, et al. (2001) Ca(2+)-sensor region of IP(3) receptor controls intracellular Ca(2+) signaling. *EMBO J* 20(7):1674–1680.
33. Tu H, et al. (2002) Functional characterization of the type 1 inositol 1,4,5-trisphosphate receptor coupling domain SII(+/-) splice variants and the Opisthotonos mutant form. *Biophys J* 82(4):1995–2004.
34. Iismaa SE, Mearns BM, Lorand L, Graham RM (2009) Transglutaminases and disease: Lessons from genetically engineered mouse models and inherited disorders. *Physiol Rev* 89(3):991–1023.
35. Eckert RL, et al. (2014) Transglutaminase regulation of cell function. *Physiol Rev* 94(2): 383–417.
36. Wilhelmus MM, van Dam AM, Drukarch B (2008) Tissue transglutaminase: A novel pharmacological target in preventing toxic protein aggregation in neurodegenerative diseases. *Eur J Pharmacol* 585(2-3):464–472.
37. Wang DS, et al. (2008) Cognitive performance correlates with cortical isopeptide immunoreactivity as well as Alzheimer type pathology. *J Alzheimers Dis* 13(1):53–66.
38. Ruan Q, Johnson GV (2007) Transglutaminase 2 in neurodegenerative disorders. *Front Biosci* 12:891–904.
39. Junn E, Ronchetti RD, Quezado MM, Kim SY, Mouradian MM (2003) Tissue transglutaminase-induced aggregation of alpha-synuclein: Implications for Lewy body formation in Parkinson's disease and dementia with Lewy bodies. *Proc Natl Acad Sci USA* 100(4):2047–2052.
40. Selkoe DJ, Abraham C, Ihara Y (1982) Brain transglutaminase: In vitro crosslinking of human neurofilament proteins into insoluble polymers. *Proc Natl Acad Sci USA* 79(19):6070–6074.
41. Kahlem P, Green H, Djian P (1998) Transglutaminase action imitates Huntington's disease: Selective polymerization of Huntingtin containing expanded polyglutamine. *Mol Cell* 1(4):595–601.
42. Bonelli RM, Aschoff A, Niederwieser G, Heuberger C, Jirikowski G (2002) Cerebrospinal fluid tissue transglutaminase as a biochemical marker for Alzheimer's disease. *Neurobiol Dis* 11(1):106–110.
43. Wilhelmus MM, et al. (2009) Transglutaminases and transglutaminase-catalyzed crosslinks colocalize with the pathological lesions in Alzheimer's disease brain. *Brain Pathol* 19(4):612–622.
44. Vermes I, Steur EN, Jirikowski GF, Haanen C (2004) Elevated concentration of cerebrospinal fluid tissue transglutaminase in Parkinson's disease indicating apoptosis. *Mov Disord* 19(10):1252–1254.
45. Johnson GV, et al. (1997) Transglutaminase activity is increased in Alzheimer's disease brain. *Brain Res* 751(2):323–329.
46. Mastroberardino PG, et al. (2002) 'Tissue' transglutaminase ablation reduces neuronal death and prolongs survival in a mouse model of Huntington's disease. *Cell Death Differ* 9(9):873–880.
47. Bailey CD, Johnson GV (2005) Tissue transglutaminase contributes to disease progression in the R6/2 Huntington's disease mouse model via aggregate-independent mechanisms. *J Neurochem* 92(1):83–92.
48. Chun W, Lesort M, Tucholski J, Ross CA, Johnson GV (2001) Tissue transglutaminase does not contribute to the formation of mutant huntingtin aggregates. *J Cell Biol* 153(1):25–34.
49. Jeitner TM, Pinto JT, Krasnikov BF, Horswill M, Cooper AJ (2009) Transglutaminases and neurodegeneration. *J Neurochem* 109(Suppl 1):160–166.
50. Akar U, et al. (2007) Tissue transglutaminase inhibits autophagy in pancreatic cancer cells. *Mol Cancer Res* 5(3):241–249.
51. D'Eletto M, et al. (2009) Transglutaminase 2 is involved in autophagosome maturation. *Autophagy* 5(8):1145–1154.
52. Kimura S, Noda T, Yoshimori T (2007) Dissection of the autophagosome maturation process by a novel reporter protein, tandem fluorescent-tagged LC3. *Autophagy* 3(5): 452–460.
53. Csosz E, et al. (2008) Substrate preference of transglutaminase 2 revealed by logistic regression analysis and intrinsic disorder examination. *J Mol Biol* 383(2):390–402.
54. Karpuj MV, et al. (2002) Prolonged survival and decreased abnormal movements in transgenic model of Huntington disease, with administration of the transglutaminase inhibitor cystamine. *Nat Med* 8(2):143–149.
55. Van Raamsdonk JM, et al. (2005) Cystamine treatment is neuroprotective in the YAC128 mouse model of Huntington disease. *J Neurochem* 95(1):210–220.
56. McConoughey SJ, et al. (2010) Inhibition of transglutaminase 2 mitigates transcriptional dysregulation in models of Huntington disease. *EMBO Mol Med* 2(9):349–370.
57. Dedeoglu A, et al. (2002) Therapeutic effects of cystamine in a murine model of Huntington's disease. *J Neurosci* 22(20):8942–8950.
58. Karpuj MV, et al. (1999) Transglutaminase aggregates huntingtin into non-amyloidogenic polymers, and its enzymatic activity increases in Huntington's disease brain nuclei. *Proc Natl Acad Sci USA* 96(13):7388–7393.
59. Krzysztoń-Russjan J, et al. (2013) A study of molecular changes relating to energy metabolism and cellular stress in people with Huntington's disease: Looking for biomarkers. *J Bioenerg Biomembr* 45(1-2):71–85.
60. Cariello L, et al. (1996) Transglutaminase activity is related to CAG repeat length in patients with Huntington's disease. *Hum Genet* 98(6):633–635.
61. Munsie L, et al. (2011) Mutant huntingtin causes defective actin remodeling during stress: Defining a new role for transglutaminase 2 in neurodegenerative disease. *Hum Mol Genet* 20(10):1937–1951.
62. Schaertl S, et al. (2010) A profiling platform for the characterization of transglutaminase 2 (TG2) inhibitors. *J Biomol Screen* 15(5):478–487.
63. Sugawara H, Kurosaki M, Takata M, Kurosaki T (1997) Genetic evidence for involvement of type 1, type 2 and type 3 inositol 1,4,5-trisphosphate receptors in signal transduction through the B-cell antigen receptor. *EMBO J* 16(11):3078–3088.
64. Zhang H, et al. (2008) Full length mutant huntingtin is required for altered Ca2+ signaling and apoptosis of striatal neurons in the YAC mouse model of Huntington's disease. *Neurobiol Dis* 31(1):80–88.
65. Tang TS, et al. (2005) Disturbed Ca2+ signaling and apoptosis of medium spiny neurons in Huntington's disease. *Proc Natl Acad Sci USA* 102(7):2602–2607.
66. Tang TS, Chen X, Liu J, Bezprozvanny I (2007) Dopaminergic signaling and striatal neurodegeneration in Huntington's disease. *J Neurosci* 27(30):7899–7910.
67. Datta S, Antonyak MA, Cerione RA (2007) GTP-binding-defective forms of tissue transglutaminase trigger cell death. *Biochemistry* 46(51):14819–14829.
68. Citron BA, SantaCruz KS, Davies PJ, Festoff BW (2001) Intron-exon swapping of transglutaminase mRNA and neuronal Tau aggregation in Alzheimer's disease. *J Biol Chem* 276(5):3295–3301.
69. Lee J, et al. (2004) Transglutaminase 2 induces nuclear factor-kappaB activation via a novel pathway in BV-2 microglia. *J Biol Chem* 279(51):53725–53735.
70. Basso M, et al. (2012) Transglutaminase inhibition protects against oxidative stress-induced neuronal death downstream of pathological ERK activation. *J Neurosci* 32(19):6561–6569.
71. Caccamo D, Currò M, Ferlazzo N, Condello S, Ientile R (2012) Monitoring of transglutaminase 2 under different oxidative stress conditions. *Amino Acids* 42(2-3): 1037–1043.
72. Yi SJ, et al. (2004) Arachidonic acid activates tissue transglutaminase and stress fiber formation via intracellular reactive oxygen species. *Biochem Biophys Res Commun* 325(3):819–826.
73. Sheline YI, et al. (2010) Amyloid plaques disrupt resting state default mode network connectivity in cognitively normal elderly. *Biol Psychiatry* 67(6):584–587.
74. Höhn S, et al. (2011) Behavioral and in vivo electrophysiological evidence for presymptomatic alteration of prefrontostriatal processing in the transgenic rat model for huntington disease. *J Neurosci* 31(24):8986–8997.
75. Sorg C, et al. (2007) Selective changes of resting-state networks in individuals at risk for Alzheimer's disease. *Proc Natl Acad Sci USA* 104(47):18760–18765.
76. Sepers MD, Raymond LA (2014) Mechanisms of synaptic dysfunction and excitotoxicity in Huntington's disease. *Drug Discov Today* 19(7):990–996.
77. Stout JC, et al. (2011) Neurocognitive signs in prodromal Huntington disease. *Neuropsychology* 25(1):1–14.
78. Fleckenstein B, et al. (2002) Gliadin T cell epitope selection by tissue transglutaminase in celiac disease. Role of enzyme specificity and pH influence on the transamidation versus deamidation process. *J Biol Chem* 277(37):34109–34116.
79. Stamnaes J, Fleckenstein B, Sollid LM (2008) The propensity for deamidation and transamidation of peptides by transglutaminase 2 is dependent on substrate affinity and reaction conditions. *Biochim Biophys Acta* 1784(11):1804–1811.
80. Uchida K, Miyauchi H, Furuichi T, Michikawa T, Mikoshiba K (2003) Critical regions for activation gating of the inositol 1,4,5-trisphosphate receptor. *J Biol Chem* 278(19): 16551–16560.
81. Nakade S, Maeda N, Mikoshiba K (1991) Involvement of the C-terminus of the inositol 1,4,5-trisphosphate receptor in Ca2+ release analysed using region-specific monoclonal antibodies. *Biochem J* 277(Pt 1):125–131.
82. Zhang S, Hisatsune C, Matsu-Ura T, Mikoshiba K (2009) G-protein-coupled receptor kinase-interacting proteins inhibit apoptosis by inositol 1,4,5-triphosphate receptor-mediated Ca2+ signal regulation. *J Biol Chem* 284(42):29158–29169.
83. Mignery GA, Südhof TC (1990) The ligand binding site and transduction mechanism in the inositol-1,4,5-triphosphate receptor. *EMBO J* 9(12):3893–3898.
84. Hamada K, Miyata T, Mayanagi K, Hirota J, Mikoshiba K (2002) Two-state conformational changes in inositol 1,4,5-trisphosphate receptor regulated by calcium. *J Biol Chem* 277(24):21115–21118.

85. Hamada K, Terauchi A, Mikoshiba K (2003) Three-dimensional rearrangements within inositol 1,4,5-trisphosphate receptor by calcium. *J Biol Chem* 278(52):52881–52889.
86. Sato C, et al. (2004) Inositol 1,4,5-trisphosphate receptor contains multiple cavities and L-shaped ligand-binding domains. *J Mol Biol* 336(1):155–164.
87. Boehning D, Joseph SK (2000) Direct association of ligand-binding and pore domains in homo- and heterotetrameric inositol 1,4,5-trisphosphate receptors. *EMBO J* 19(20): 5450–5459.
88. Schug ZT, Joseph SK (2006) The role of the S4-S5 linker and C-terminal tail in inositol 1,4,5-trisphosphate receptor function. *J Biol Chem* 281(34):24431–24440.
89. Chan J, et al. (2010) Structural studies of inositol 1,4,5-trisphosphate receptor: Coupling ligand binding to channel gating. *J Biol Chem* 285(46):36092–36099.
90. Rossi AM, et al. (2009) Synthetic partial agonists reveal key steps in IP3 receptor activation. *Nat Chem Biol* 5(9):631–639.
91. Hamada K, Mikoshiba K (2012) Revisiting channel allostery: A coherent mechanism in $IP_3$ and ryanodine receptors. *Sci Signal* 5(225):pe24.
92. Sayers LG, et al. (1997) Intracellular targeting and homotetramer formation of a truncated inositol 1,4,5-trisphosphate receptor-green fluorescent protein chimera in Xenopus laevis oocytes: Evidence for the involvement of the transmembrane spanning domain in endoplasmic reticulum targeting and homotetramer complex formation. *Biochem J* 323(Pt 1):273–280.
93. Nakayama T, et al. (2004) The regulatory domain of the inositol 1,4,5-trisphosphate receptor is necessary to keep the channel domain closed: Possible physiological significance of specific cleavage by caspase 3. *Biochem J* 377(Pt 2):299–307.
94. Anyatonwu G, Joseph SK (2009) Surface accessibility and conformational changes in the N-terminal domain of type I inositol trisphosphate receptors: Studies using cysteine substitution mutagenesis. *J Biol Chem* 284(12):8093–8102.
95. Anyatonwu G, et al. (2010) Calcium-dependent conformational changes in inositol trisphosphate receptors. *J Biol Chem* 285(32):25085–25093.
96. Shinohara T, et al. (2011) Mechanistic basis of bell-shaped dependence of inositol 1,4,5-trisphosphate receptor gating on cytosolic calcium. *Proc Natl Acad Sci USA* 108(37): 15486–15491.
97. Maeda N, et al. (1991) Structural and functional characterization of inositol 1,4,5-trisphosphate receptor channel from mouse cerebellum. *J Biol Chem* 266(2):1109–1116.
98. Nakamura K, et al. (2013) Distinct roles of M1 and M3 muscarinic acetylcholine receptors controlling oscillatory and non-oscillatory [Ca] increase. *Cell Calcium* 54(2): 111–119.